

# CALIPSO Browse Image Tutorial

## Introduction

This document describes the interpretation of CALIPSO’s standard suite of data product browse images.

CALIP is an elastic backscatter lidar that emits pulsed laser light and measures the energies scattered directly back to the satellite from molecules and particulates (i.e. aerosols, clouds) in the atmosphere. CALIP is a three-channel instrument operating at two wavelengths: 532 nm and 1064 nm. In the CALIP receiver, the 532 nm backscatter is decomposed into polarization planes parallel (||) and perpendicular (⊥) to the polarization plane of the transmitted laser light. Figure 1 shows a functional diagram of the lidar receiver system. The blocks labeled “Detectors and Electronics” are what will be referred to as “detectors”.

Once the signals have been range-scaled, energy and gain normalized, geolocated and altitude registered, and calibrated, the measured backscatter from each detector can be expressed by the following equations:

$$\beta'_{532,||}(z) = \beta_{532,||}(z)T^2_{532}(z) \quad (1)$$

$$\beta'_{532,\perp}(z) = \beta_{532,\perp}(z)T^2_{532}(z) \quad (2)$$

$$\beta'_{1064}(z) = \beta_{1064}(z)T^2_{1064}(z) \quad (3)$$

In equations 1-3,  $\beta'_\lambda(z)$  is the attenuated backscatter at wavelength  $\lambda$ ,  $\beta_\lambda(z)$  is the volume backscatter coefficient, and  $T^2_\lambda$  is the two-way transmittance between the laser and the sample volume.

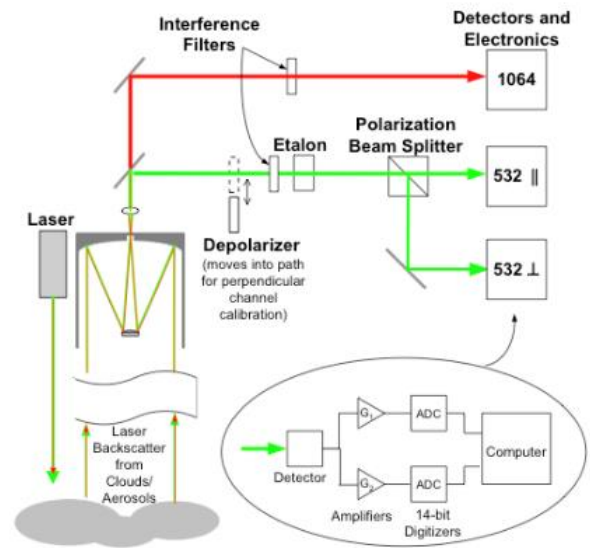


Figure 1: CALIP detector and electronics block diagram.

## CALIP Images

A review of each of the generated CALIP browse images is summarized below, focusing on a night-time orbital segment on April 15, 2010 from the V5.00 Lidar Level 1 and Level 2 data release.

CALIPSO browse images for several key observables are reproduced using colormaps that improve accessibility for individuals with color vision deficiencies (CVD; Vaillant de Guélis et al., 2025). In some instances, (Depolarization and Attenuated Color Ratios), these new color maps universally replace the color maps used in previous versions. Two versions of browse images (legacy and CVD-accessible) are provided for the 532 nm and 1064 nm the total attenuated backscatter coefficients. The new attenuated backscatter colormap builds upon the strengths of the legacy colormap. It retains three backscattering regimes (clouds, aerosols, and clear skies) to resolve detail within the range of magnitudes required for scientific interpretation. Similar colors are used, but green is eliminated to avoid red-green ambiguities for individuals with CVD. Transitions between the three regimes are softened to reduce the appearance of false boundaries in the atmosphere that were prevalent in the legacy colormap. Lastly, the lower backscatter limit is reduced by an order of magnitude, allowing weakly backscattering particulate features to be resolved from the molecular background, particularly in the 532 nm perpendicular channel browse images.

## Total 532 nm Attenuated Backscatter

Figure 2 (legacy) and Figure 3 (CVD-accessible) show the total 532 nm attenuated backscatter signals, the sum of the 532 nm parallel and perpendicular return signals, as defined in equation 4.

$$\beta'_{532}(z) = [\beta_{532,\parallel}(z) + \beta_{532,\perp}(z)]T^2_{532}(z) \quad (4)$$

The signal strength has been color coded such that blues correspond to molecular scattering and weak aerosol scattering, aerosols generally show up as yellow/red/orange. Stronger cloud signals are plotted in gray scales, while weaker cloud returns are similar in strength to strong aerosol returns and coded in yellows and reds.

The CALIOP browse images use this unique color scale, and not some generic color scale, because CALIOP data has significantly lower signal-to-noise ratio (SNR) compared to most ground-based or aircraft instruments. The CALIOP color scale has been specifically designed to allow data users to easily pick out and discern features of interest from the molecular backscatter signal and noise fluctuations.

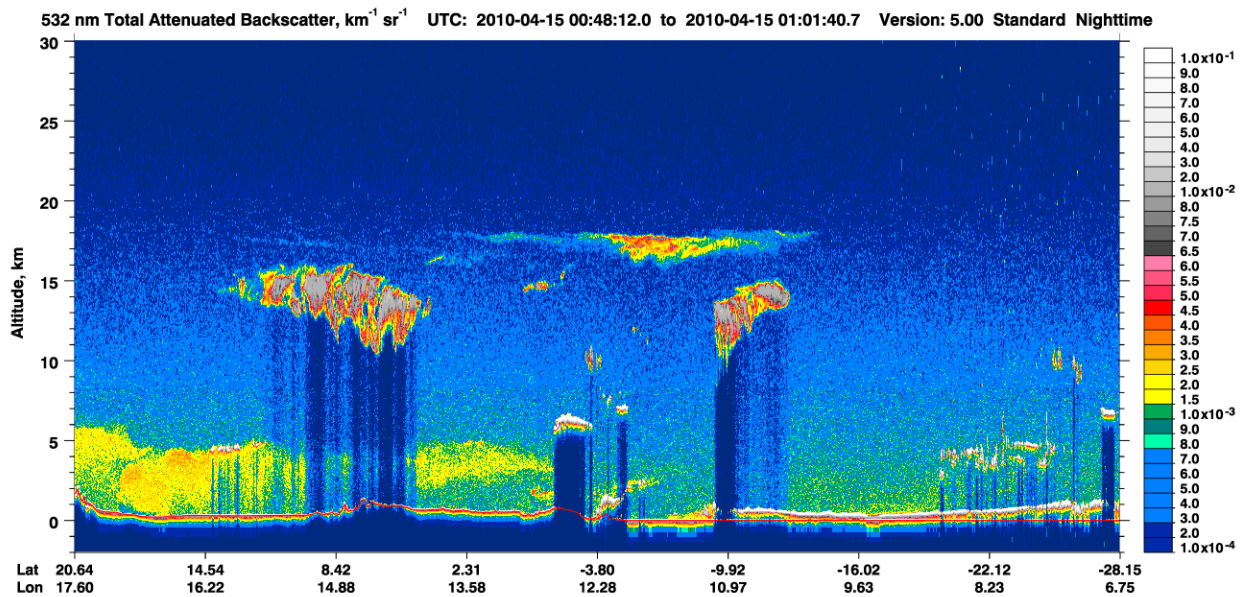


Figure 2: 532 nm Total Attenuated Backscatter using the legacy CALIOP color map. The nighttime orbital segment is from April 15th, 2010 between 00:48:12Z to 01:01:40Z.

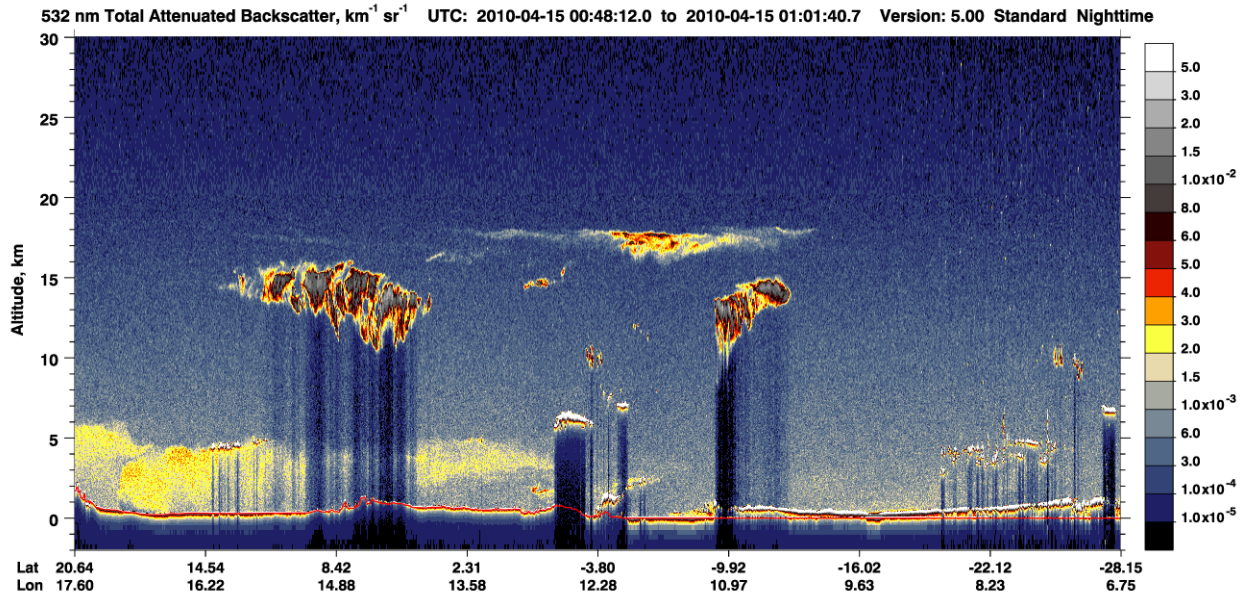


Figure 3: 532 nm Total Attenuated Backscattering using the color-vision-deficiency-accessible color map. The nighttime orbital segment is from April 15th, 2010 between 00:48:12Z to 01:01:40Z.

### Perpendicular 532 nm Attenuated Backscatter

Figure 4 (legacy) and Figure 5 (CVD-accessible) show the 532 nm attenuated perpendicular backscatter signal, as defined in equation 2.

The 532 nm attenuated perpendicular backscatter quantifies the contributions from backscattered photons for which the polarization state has been changed from that of the linearly polarized beam emitted by the laser. These changes in polarization state are useful for distinguishing between backscatter from non-spherical particles (e.g., dust and ice crystals), which induce a change of state, and spherical particles (e.g., liquid droplets), which typically do not induce a change. However, because the receiver footprint of the lidar is large ( $\sim 90$  m), multiple scattering of photons backscattered from optically thick layers of liquid droplets (e.g., cumulus and stratus clouds) can create large perpendicular channel backscatter signals that increase as a function of layer penetration depth. So, it is common to see a significant perpendicular backscatter return from dense water clouds.

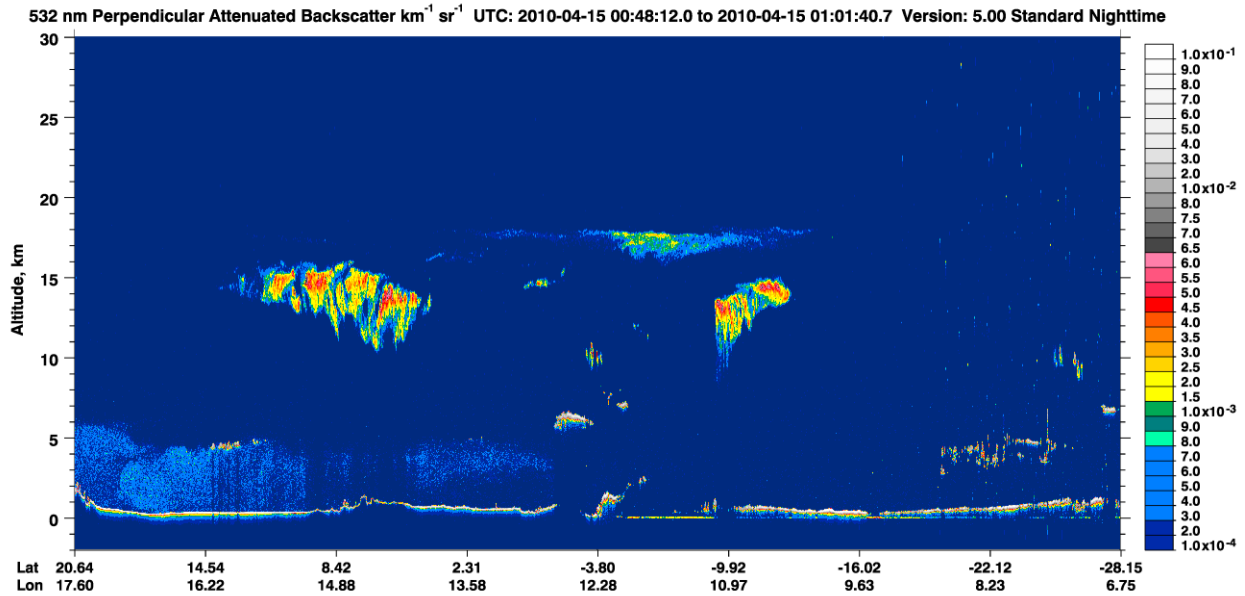


Figure 4: 532 nm Perpendicular Attenuated Backscatter using the legacy CALIOP color map. The nighttime orbital segment is from April 15th, 2010 between 00:48:12Z to 01:01:40Z.

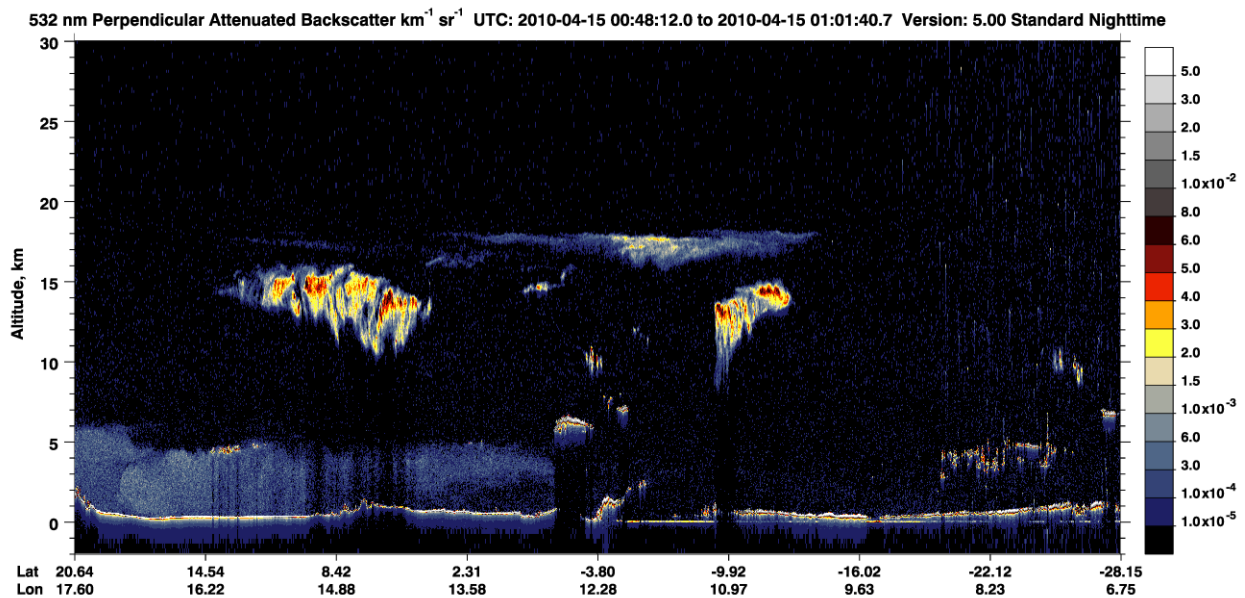


Figure 5: 532 nm Perpendicular Attenuated Backscatter using the color-vision-deficiency-accessible color map. The nighttime orbital segment is from April 15th, 2010 between 00:48:12Z to 01:01:40Z.

### Depolarization Ratio 532 nm

Figure 6 shows the volume depolarization ratio, the ratio of the 532 nm perpendicular and parallel attenuated backscatter, as defined in equation 5.

$$\delta_v(z) = \frac{\beta'_{532,\perp}(z)}{\beta'_{532,\parallel}(z)} \quad (5)$$

This volume depolarization ratio is useful for discerning the difference between spherical and non-spherical particles. Non-spherical particles (i.e. dust, ice crystals) will change the polarization state of the backscattered light, while spherical particles such as water droplets or spherical aerosols will not.

Ice clouds (e.g., cirrus) generally exhibit volume depolarization ratios in the 0.25-0.45 range ([Kikuchi et al., 2021](#)), while dust aerosol depolarization ratios are usually in the 0.20 to 0.3 range ([Liu et al., 2011](#)), with lower values expected in faint, weakly scattering layers. Water clouds will exhibit an increase in depolarization ratio as a function of the penetration depth, due to the contribution of multiple scattering. Layer-integrated volume depolarizations for opaque water clouds are typically  $0.21 \pm 0.06$  ([Young et al., 2018](#)).

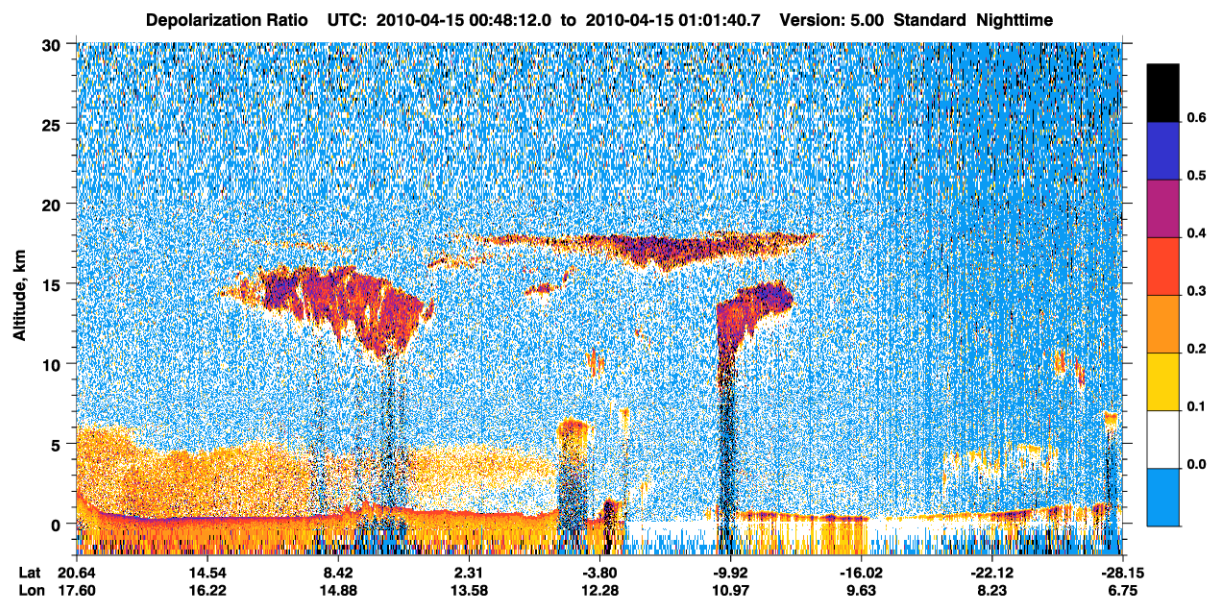


Figure 6: 532 nm Depolarization Ratio. The nighttime orbital segment is from April 15th, 2010 between 00:48:12Z to 01:01:40Z.

### Total 1064 nm Attenuated Backscatter

Figure 7 (legacy) and Figure 8 (CVD-accessible) show the total 1064 nm attenuated backscatter signal. As shown earlier in Figure 1, CALIOP does not separate the 1064 nm signal into perpendicular and parallel components.

The 1064 nm attenuated backscatter image can be useful for picking out faint (weak) scattering layers because the molecular backscatter is virtually non-existent. Also, looking for differences in the 532 nm and 1064 nm attenuated backscatter is useful for inferring information about the particle size.

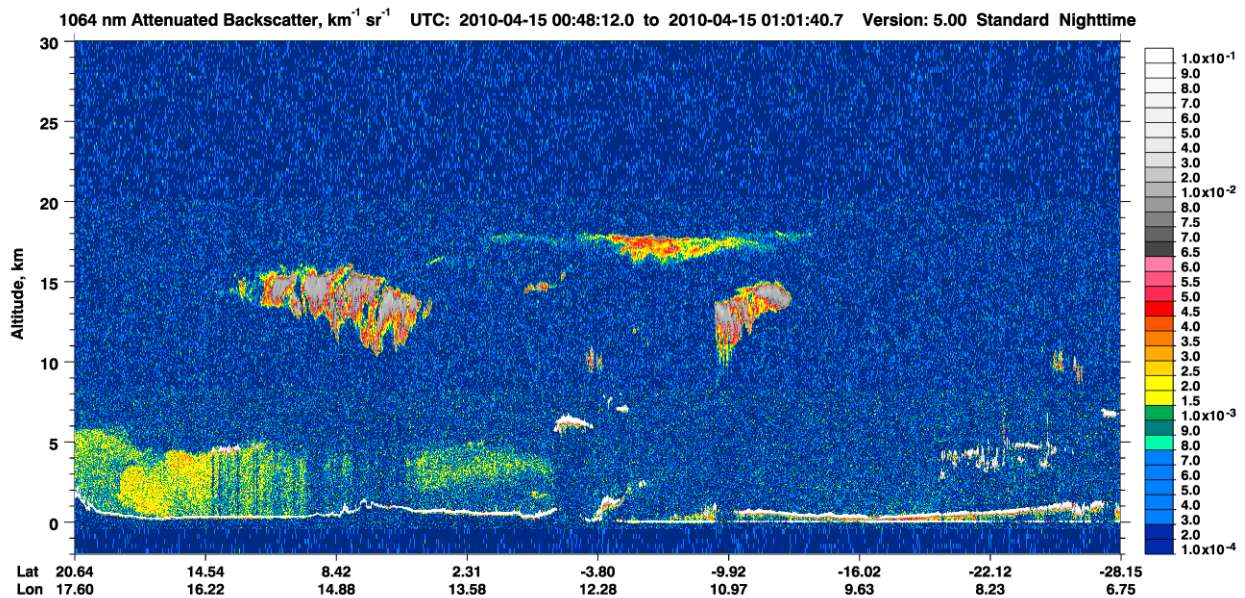


Figure 7: 1064 nm Attenuated Backscatter. The nighttime orbital segment is from April 15th, 2010 between 00:48:12Z to 01:01:40Z.

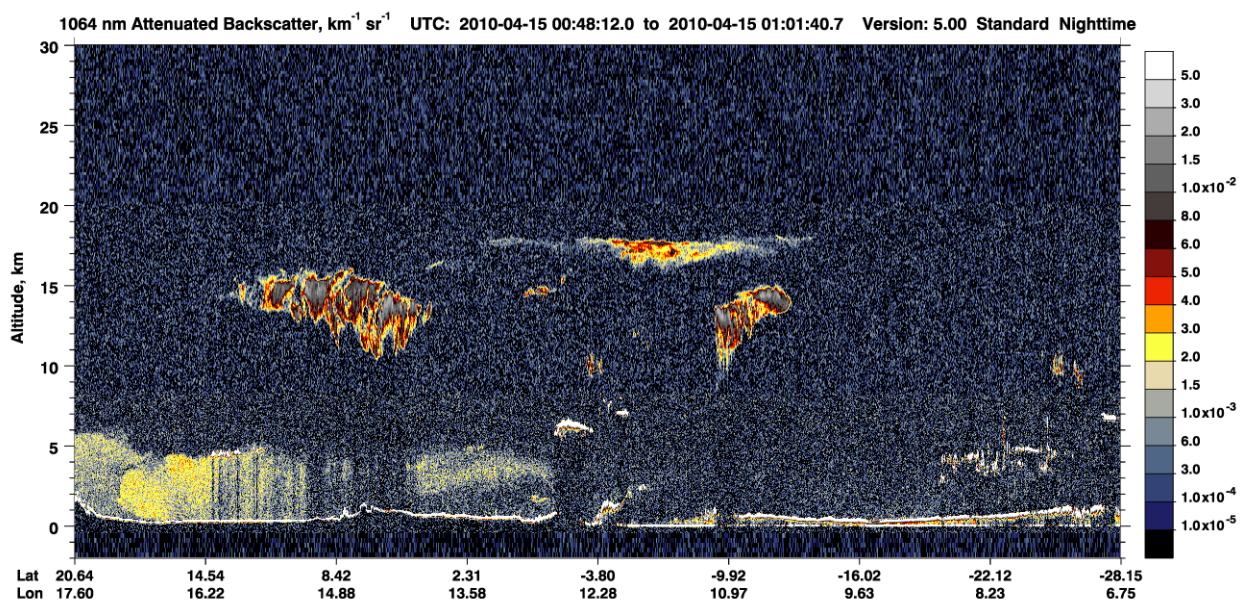


Figure 8: 1064 nm Attenuated Backscatter using the color-vision-deficiency-accessible colormap. The nighttime orbital segment is from April 15th, 2010 between 00:48:12Z to 01:01:40Z.

### Total Attenuated Backscatter Color Ratio

Figure 9 shows the total attenuated backscatter color ratio, the ratio of the 1064 nm and 532 nm backscatter, as defined in equation 6.

$$\chi'(z) = \frac{\beta'_{1064}(z)}{\beta'_{532}(z)} \quad (6)$$

The total attenuated backscatter color ratio is useful for inferring information about the size of the particles in the scattering volume. Because the backscatter coefficients are typically smaller at 1064 nm compared to 532 nm for small particles (e.g., aerosols), aerosol color ratios will often be less than 1.  $\chi'(z)$  for cirrus clouds is  $\sim 1$  and  $\sim 1.2$  for dense water clouds (Vaughan et al., 2019). Layers having particulate extinction coefficients that are much larger at 532 nm than at 1064 nm (e.g., smoke) frequently show strong vertical gradients in  $\chi'(z)$ , with low values at layer top and much larger values at layer base. When not opaque, these features typically generate unusually large color ratios within any underlying layers.

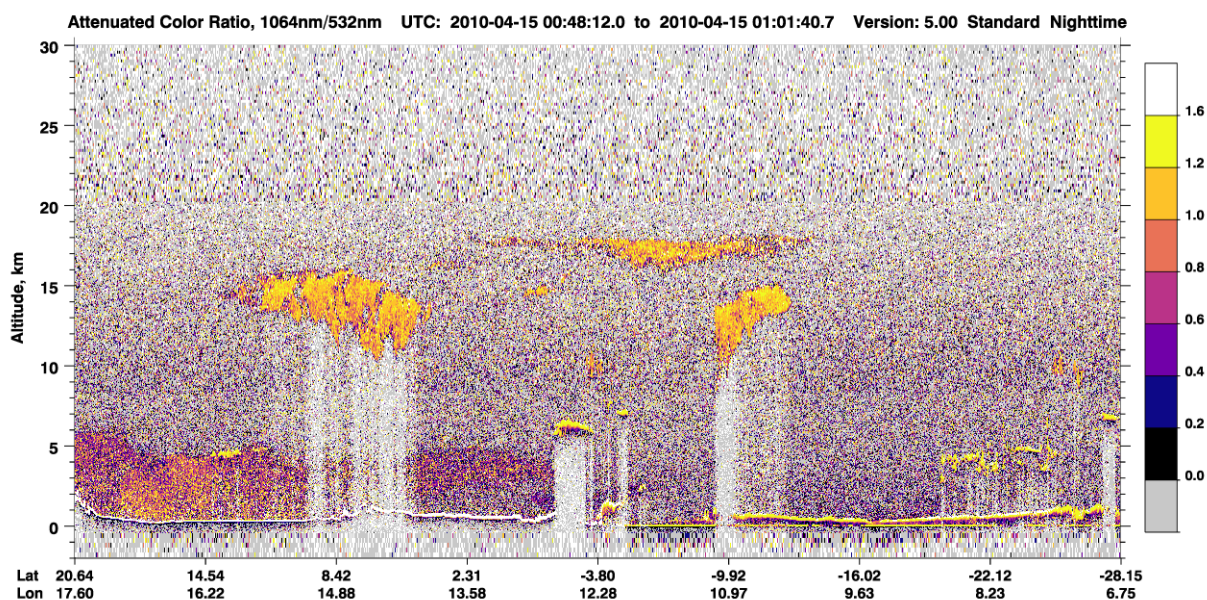


Figure 9: Attenuated Color Ratio. The nighttime orbital segment is from April 15th, 2010 between 00:48:12Z to 01:01:40Z.

### Attenuated Backscatter with Ancillary Information

Figure 10 overlays pressure, potential temperature, temperature, and tropopause height contours onto the 532 nm total attenuated backscatter. Pressure, temperature, and tropopause height are extracted from the MERRA-2 meteorological data reported in the lidar level 1 data files, while the potential temperature is computed.

Coincident browse images of CloudSat radar reflectivity (Figure 11) and cloud mask (Figure 12) are overlaid onto the 532 nm total attenuated backscatter. The CloudSat data is taken from the most recent version of the 2B-GEOPROF data products for both day and night browse images from June 2006 to April 2011. Combined nighttime images are not available after April 2011, as a battery anomaly limited CloudSat to daytime measurements only from November 2011 onward. These CALIPSO browse images are only generated when the CloudSat data is processed and publicly available, and only through August 26, 2020, after-which CloudSat was no longer in formation with CALIPSO.

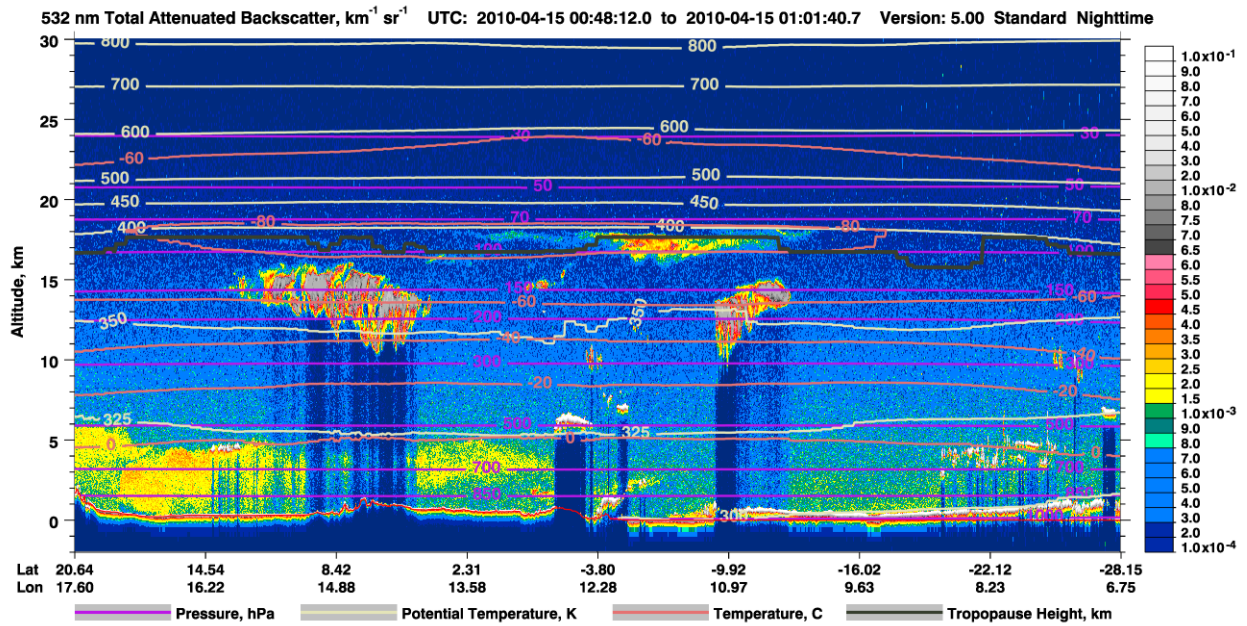


Figure 10: 532 nm Total Attenuated Backscatter overlaid with Pressure, Potential Temperature, Temperature, and Tropopause Height. The nighttime orbital segment is from April 15th, 2010 between 00:48:12Z to 01:01:40Z.

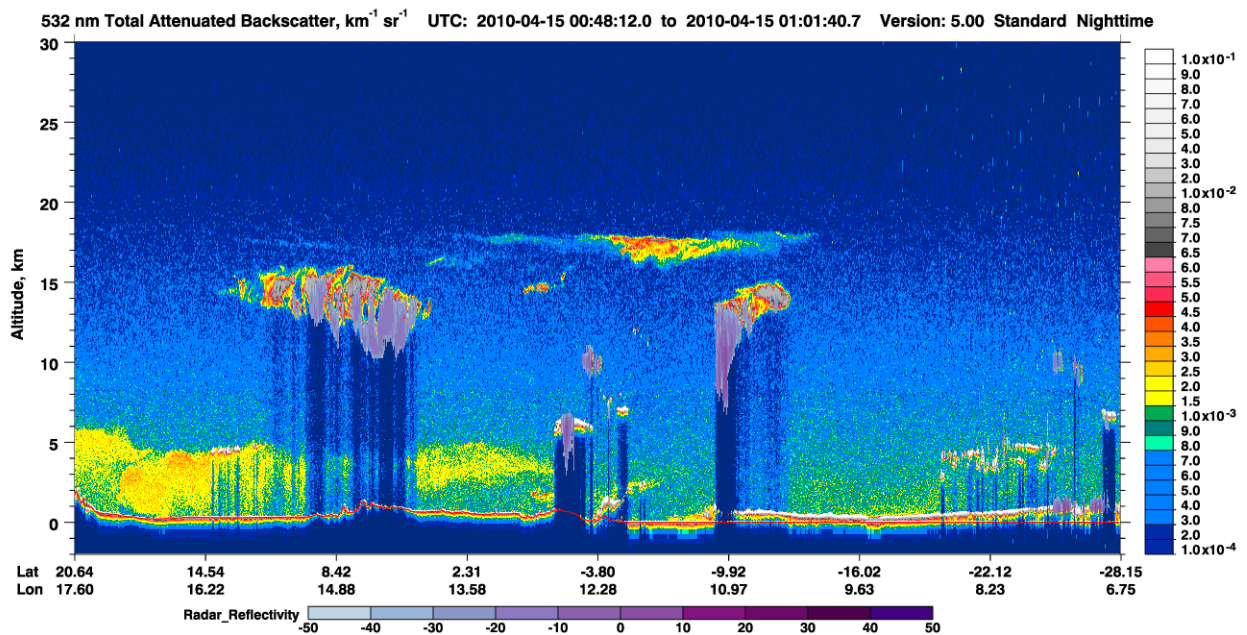


Figure 11: 532 nm Total Attenuated Backscatter overlaid with CloudSat Radar Reflectivity. The nighttime orbital segment is from April 15th, 2010 between 00:48:12Z to 01:01:40Z.

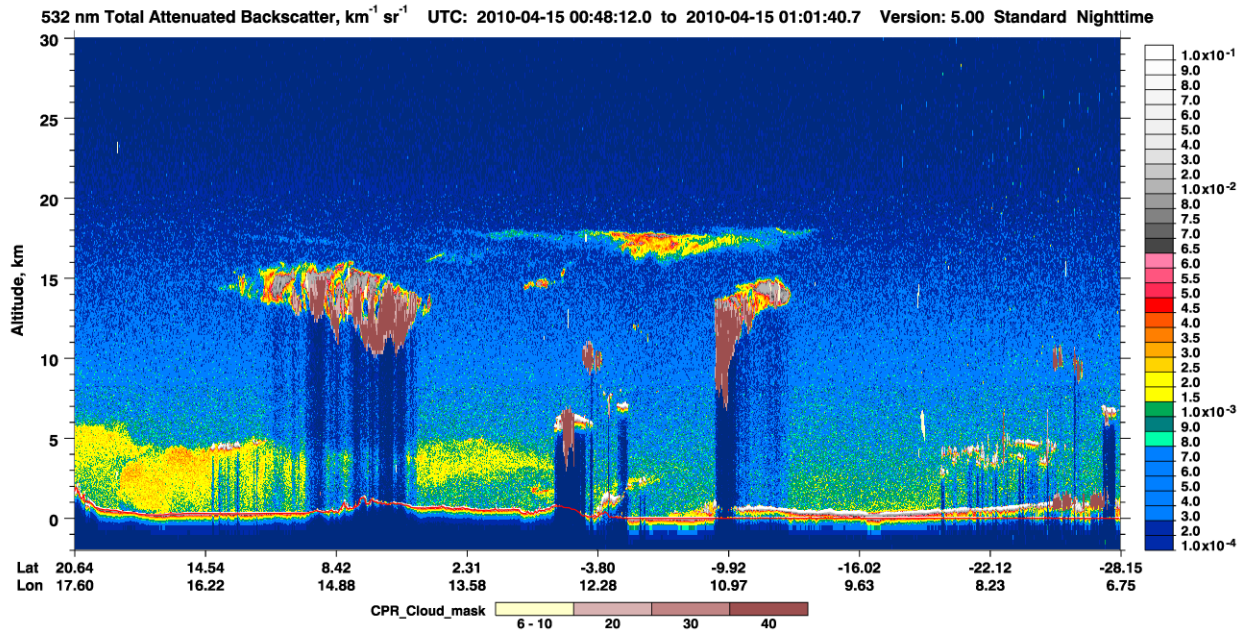


Figure 12: 532 nm Total Attenuated Backscatter with CloudSat Cloud Profiling Radar (CPR) Cloud Mask overlaid. The nighttime orbital segment is from April 15th, 2010 between 00:48:12Z to 01:01:40Z.

### Vertical Feature Mask

The following figures are colloquially known as vertical feature masks (VFM) that show the vertical and horizontal locations and types of all features, as well as some defining characteristics that make up these features. All images below are generated from the V5.00 Lidar Level 2 VFM product, contained and decoded from the *Feature\_Classification\_Flag* science data set.

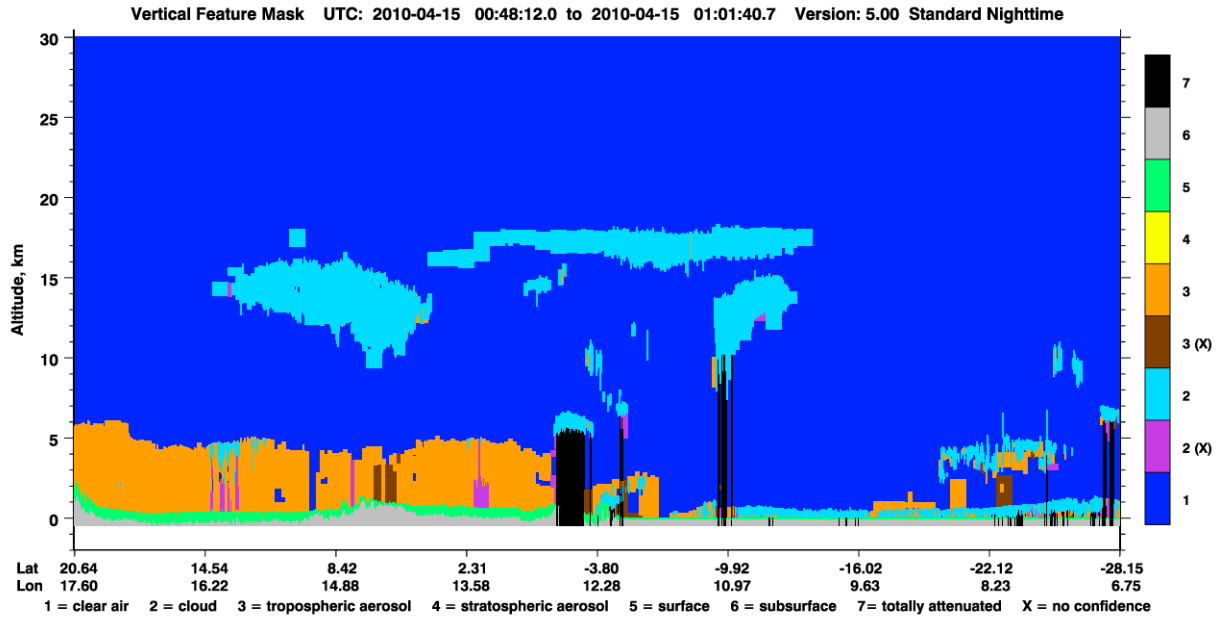


Figure 13: Layer Type, depicting the location and classification (e.g., cloud, tropospheric aerosol, surface, etc.) for each layer identified in the lidar level 2 data processing. The nighttime orbital segment is from April 15th, 2010 between 00:48:12Z to 01:01:40Z.

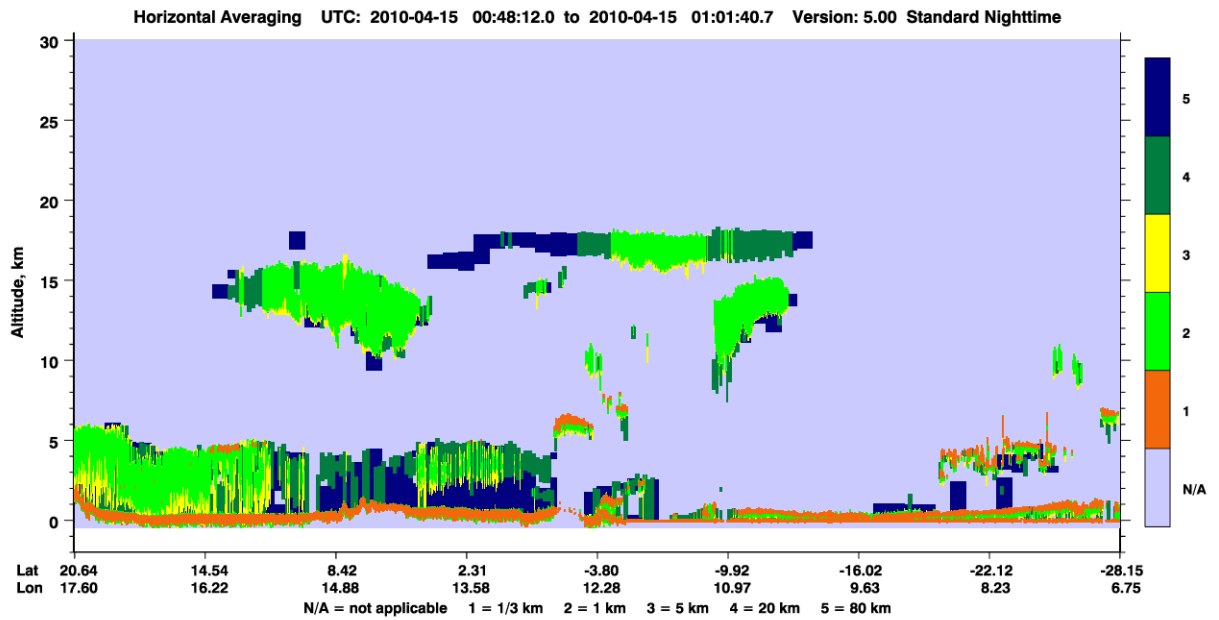


Figure 14: Horizontal averaging (from 1/3 km to 80 km) required for feature detection, based on CALIPSO's multi-gridded averaging scheme (Vaughan et al., 2009). The nighttime orbital segment is from April 15th, 2010 between 00:48:12Z to 01:01:40Z.

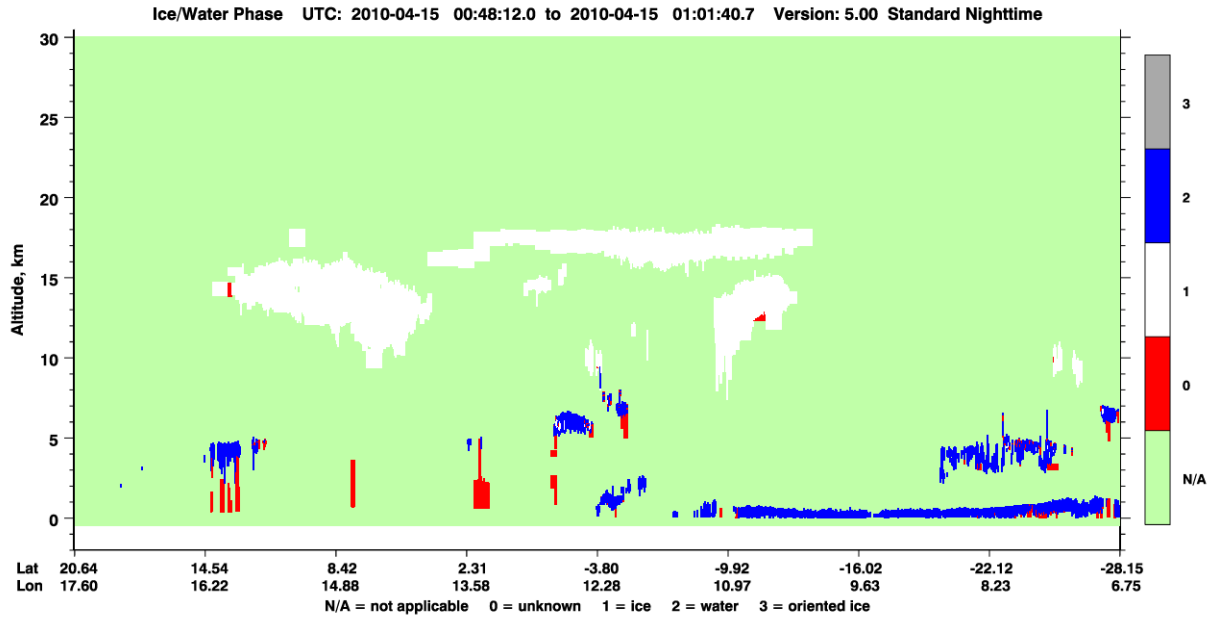


Figure 15: Ice/Water Phase for all clouds detected in the scene. The cloud phase algorithm classifies detected cloud layers as water, randomly-oriented ice (ROI), or horizontally-oriented ice (HOI) based on relations between depolarization, backscatter, and color ratio (Hu et al., 2009, Avery et al., 2020). The nighttime orbital segment is from April 15th, 2010 between 00:48:12Z to 01:01:40Z.

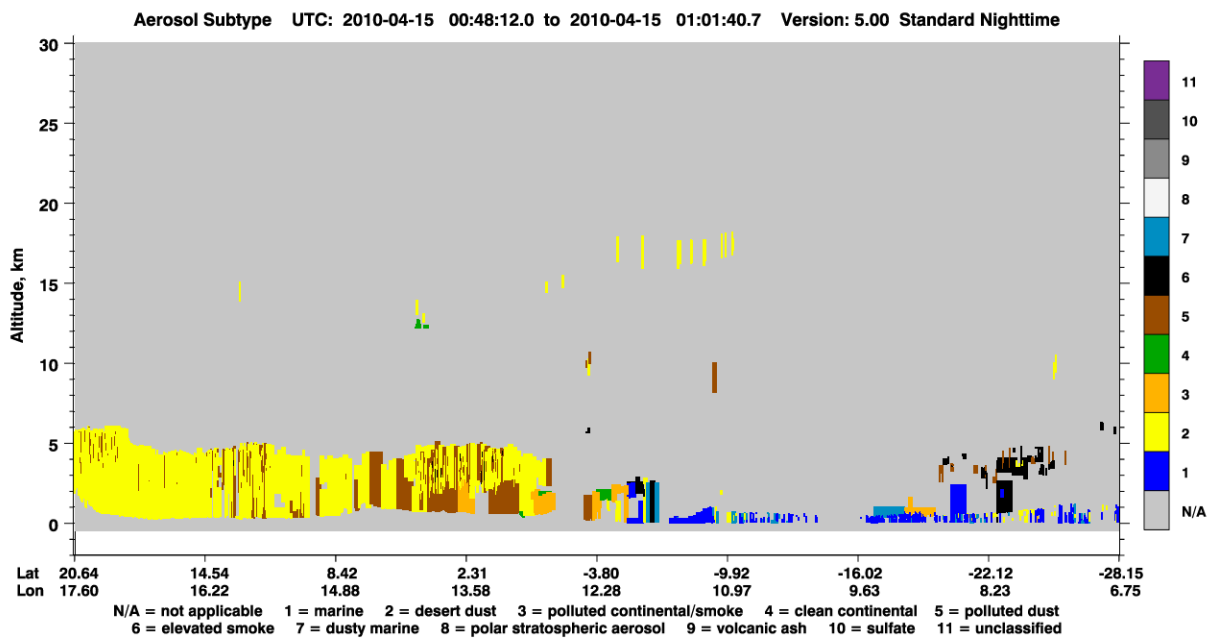


Figure 16: Aerosol subtype for all tropospheric and stratospheric aerosol layers detected in the scene, based on output from the aerosol classification algorithms (Kim et al., 2018; Tackett et al., 2023). The nighttime orbital segment is from April 15th, 2010 between 00:48:12Z to 01:01:40Z.

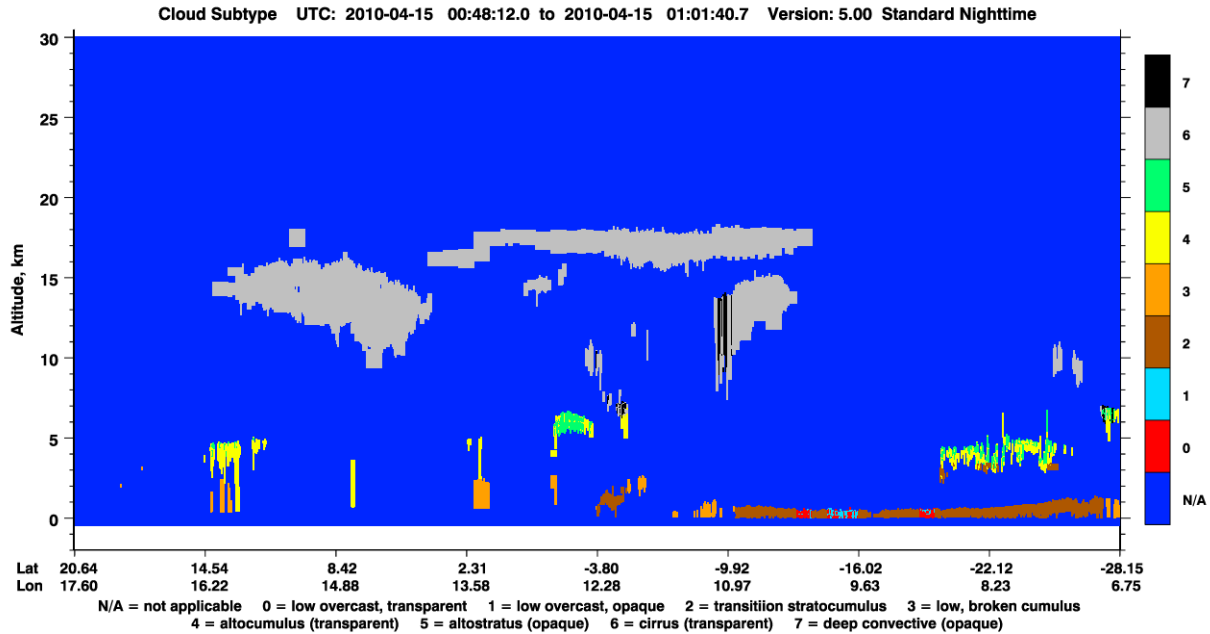


Figure 17: Cloud subtype for all cloud layers in the scene, based on output from the cloud classification algorithm. The nighttime orbital segment is from April 15th, 2010 between 00:48:12Z to 01:01:40Z.

## IIR Images

The CALIPSO Imaging Infrared Radiometer (IIR) provides observations at 1-km resolution in three channels centered at 8.65, 10.6, and 12.05  $\mu\text{m}$ . The swath is 69-km wide and is centered on the CALIOP track. Brightness temperatures reported in the Version 4 IIR Level 2 swath product are derived from the calibrated radiances reported in the Version 2 IIR Level 1 product using the relationships detailed in [Garnier et al. \(2018\)](#).

Figure 18 (top) shows brightness temperatures at 12.05  $\mu\text{m}$ . In clear sky conditions, IIR channels see the surface and observed brightness temperatures are typically only several degrees colder than the surface. Clouds (and some absorbing aerosols) in the atmospheric column usually reduce the brightness temperature compared to clear sky conditions. The amplitude of this reduction increases as cloud altitude increases (for a given optical depth) and as effective emissivity (or optical depth) increases for a given altitude.

Figure 18 (middle and bottom) shows brightness temperature difference between channels 8.65 and 12.05  $\mu\text{m}$ , and between channels 10.6 and 12.05  $\mu\text{m}$ , respectively. In clear sky conditions, inter-channel brightness temperature differences are due to different atmospheric absorptions and surface properties and can be either positive or negative. These images are useful to identify the presence of small cloud crystals or water droplets, which induce large positive inter-channel brightness temperature differences sometimes exceeding +10 K.

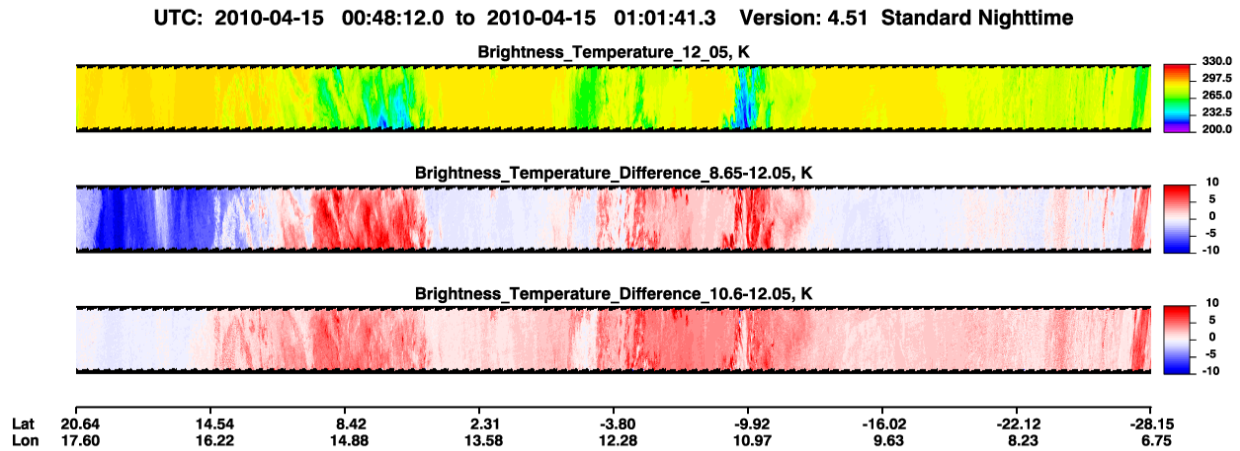


Figure 18: CALIPSO Imaging Infrared Radiometer (IIR) brightness temperature and brightness temperature differences. The nighttime orbital segment is from April 15th, 2010 between 00:48:12Z to 01:01:40Z.

## WFC Images

The CALIPSO Wide Field Camera (WFC) is a narrow-band push-broom imager that provides continuous high spatial resolution (125m) images of radiance and reflectance during the daylight segments of a CALIPSO orbit over a 61 km swath centered on the lidar footprint. The spectral band of the WFC is designed to match the Aqua MODIS instrument channel 1 having a central wavelength of 645 nm and a bandwidth of 50 nm. Figure 19 shows a WFC image but does correspond with the other images in this document as it is collected on the next daytime orbit.

The CALIPSO WFC stopped operation on April 11, 2020.

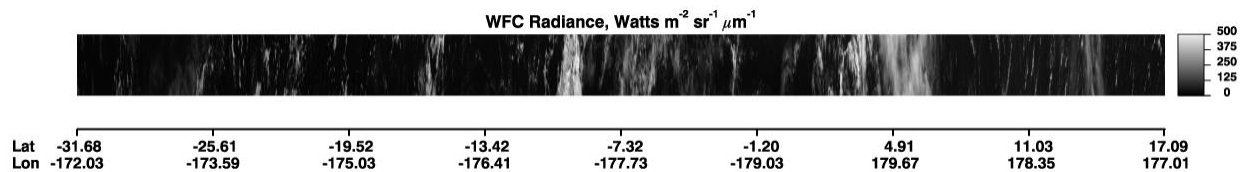


Figure 19: CALIPSO Wide Field Camera (WFC) radiance image. The daytime orbital segment is from April 15<sup>th</sup>, 2010 between 01:34:38Z to 01:48:08Z.

## References

- Avery, M., R. Ryan, B. Getzewich, M. Vaughan, D. Winker, Y. Hu, A. Garnier, J. Pelon, and C. Verhappen, 2020: CALIOP V4 cloud thermodynamic phase assignment and the impact of near-nadir viewing angles, *Atmos. Meas. Tech.*, **13**, 4539-4563, <https://doi.org/10.5194/amt-13-4539-2020>.
- Garnier, A., T. Tremas, J. Pelon, K.-P. Lee, D. Nobileau, L. Gross-Colzy, N. Pascal, P. Ferrage, and N. A. Scott, 2018: CALIPSO IIR Version 2 Level 1b calibrated radiances: analysis and reduction of residual biases in the Northern Hemisphere, *Atmos. Meas. Tech.*, **11**, 2485-2500, <https://doi.org/10.5194/amt-11-2485-2018>.

- Hu, Y. D. Winker, M. Vaughan, B. Lin, A. Omar, C. Trepte, D. Flittner, P. Yang, S. L. Nasiri, B. Baum, R. Holz, W. Sun, Z. Liu, Z. Wang, S. Young, K. Stamnes, J. Huang, and R. Kuehn, 2009: CALIPSO/CALIOP Cloud Phase Discrimination Algorithm, *J. Atmos. Oceanic Technol.*, **26**, 2293–2309, <https://doi.org/10.1175/2009JTECHA1280.1>.
- Kikuchi, M., H. Okamoto, and K. Sato, 2021: A climatological view of horizontal ice plates in clouds: Findings from nadir and off-nadir CALIPSO observations, *J. Geophys. Res. Atmos.*, **126**, e2020JD033562, <https://doi.org/10.1029/2020JD033562>.
- Kim, M.-H., A. H. Omar, J. L. Tackett, M. A. Vaughan, D. M. Winker, C. R. Trepte, Y. Hu, Z. Liu, L. R. Poole, M. C. Pitts, J. Kar, and B. E. Magill, 2018: The CALIPSO Version 4 Automated Aerosol Classification and Lidar Ratio Selection Algorithm, *Atmos. Meas. Tech.*, **11**, 6107–6135, <https://doi.org/10.5194/amt-11-6107-2018>.
- Liu, Z., D. Winker, A. Omar, M. Vaughan, C. Trepte, Y. Hu, K. Powell, W. Sun, B. Lin, 2011: Effective lidar ratios of dense dust layers over North Africa derived from the CALIOP measurements, *JQSRT*, **112**, 204–213, <https://doi.org/10.1016/j.jqsrt.2010.05.006>.
- Tackett, J. L., J. Kar, M. A. Vaughan, B. Getzewich, M.-H. Kim, J.-P. Vernier, A. H. Omar, B. Magill, M. C. Pitts, and D. Winker, 2023: The CALIPSO version 4.5 stratospheric aerosol subtyping algorithm, *Atmos. Meas. Tech.*, **16**, 745–768, <https://doi.org/10.5194/amt-16-745-2023>.
- Vaillant de Guélis, T., J. L. Tackett, and D. M. Winker, 2025: A proposal for improved colorbars for cloud and aerosol lidar parameters, [31<sup>st</sup> International Laser Radar Conference](#), 23–28 June 2024, Landshut, Bavaria, Germany.
- Vaughan, M., K. Powell, R. Kuehn, S. Young, D. Winker, C. Hostetler, W. Hunt, Z. Liu, M. McGill, and B. Getzewich, 2009: Fully Automated Detection of Cloud and Aerosol Layers in the CALIPSO Lidar Measurements, *J. Atmos. Oceanic Technol.*, **26**, 2034–2050, <https://doi.org/10.1175/2009JTECHA1228.1>.
- Vaughan, M., A. Garnier, D. Josset, M. Avery, K.-P. Lee, Z. Liu, W. Hunt, J. Pelon, Y. Hu, S. Burton, J. Hair, J. Tackett, B. Getzewich, J. Kar, and S. Rodier, 2019: “CALIPSO Lidar Calibration at 1064 nm: Version 4 Algorithm”, *Atmos. Meas. Tech.*, **12**, 51–82, <https://doi.org/10.5194/amt-12-51-2019>.
- Young, S. A., M. A. Vaughan, J. L. Tackett, A. Garnier, J. B. Lambeth, and K. A. Powell, 2018: Extinction and Optical Depth Retrievals for CALIPSO’s Version 4 Data Release, *Atmos. Meas. Tech.*, **11**, 5701–5727, <https://doi.org/10.5194/amt-11-5701-2018>.

## Appendix A – Color Tables

The following tables provide the RGB colormaps for each of the noted CALIOP browse images.

Table 1A: Attenuated Backscatter ( $\text{km}^{-1}\text{sr}^{-1}$ ) for Figure 2, Figure 4, Figure 7, Figure 10, Figure 11, and Figure 12. Missing data is plotted in black.

Minimum	Maximum	R	G	B
-Inf	<1e-4	0	42	127
1e-4	2e-4	0	42	170
2e-4	3e-4	0	42	170
3e-4	4e-4	0	127	255
4e-4	5e-4	0	127	255
5e-4	6e-4	0	127	255

Minimum	Maximum	R	G	B
6e-4	7e-4	0	127	255
7e-4	8e-4	0	127	255
8e-4	9e-4	0	255	170
9e-4	1e-3	0	127	127
1.0e-3	1.5e-3	0	170	85
1.5e-3	2.0e-3	255	255	0
2.0e-3	2.5e-3	255	255	0
2.5e-3	3.0e-3	255	212	0
3.0e-3	3.5e-3	255	170	0
3.5e-3	4.0e-3	255	127	0
4.0e-3	4.5e-3	255	85	0
4.5e-3	5.0e-3	255	0	0
5.0e-3	5.5e-3	255	42	85
5.5e-3	6.0e-3	255	85	127
6.0e-3	6.5e-3	255	127	170
6.5e-3	7.0e-3	70	70	70
7.0e-3	7.5e-3	100	100	100
7.5e-3	8.0e-3	130	130	130
8e-3	1e-2	155	155	155
1e-2	2e-2	180	180	180
2e-2	3e-2	200	200	200
3e-2	4e-2	225	225	225
4e-2	5e-2	235	235	235
5e-2	6e-2	240	240	240
6e-2	7e-2	242	242	242
7e-2	8e-2	245	245	245
8e-2	9e-2	249	249	249
9e-2	1e-1	253	253	253
1e-1	+Inf	253	255	255

Table 2A: Attenuated Backscatter ( $\text{km}^{-1}\text{sr}^{-1}$ ), color vision deficiency accessible, for Figure 3, Figure 5, and Figure 8. Missing data is plotted in black.

Minimum	Maximum	R	G	B
-Inf	<1e-5	0	0	0
1e-5	1e-4	30	31	100
1e-4	3e-4	52	67	118
3e-4	6e-4	79	102	135
6e-4	1e-3	120	136	149
1e-3	1.5e-3	167	170	160
1.5e-3	2e-3	233	218	174
2e-3	3e-3	251	255	65
3e-3	4e-3	254	161	0
4e-3	5e-3	236	36	1
5e-3	6e-3	132	17	12
6e-3	8e-3	43	0	0

Minimum	Maximum	R	G	B
8e-3	1e-2	68	59	59
1e-2	1.5e-2	96	96	96
1.5e-2	2e-2	133	133	133
2e-2	3e-2	172	172	172
3e-2	5e-2	213	213	213
5e-2	+Inf	255	255	255

Table 3A: Color Ratio for Figure 9. Missing data is plotted in black.

Minimum	Maximum	R	G	B
-Inf	0.0	200	200	200
0.0	0.2	0	0	0
0.2	0.4	13	8	135
0.4	0.6	113	0	168
0.6	0.8	186	51	136
0.8	1.0	233	114	87
1.0	1.2	253	194	41
1.2	1.6	240	249	33
1.6	+Inf	255	255	255

Table 4A: Depolarization Ratio for Figure 6. Missing data is plotted in black.

Minimum	Maximum	R	G	B
-Inf	0	10	155	244
0.0	0.1	255	255	255
0.1	0.2	255	211	9
0.2	0.3	255	150	27
0.3	0.4	255	70	39
0.4	0.5	180	35	126
0.5	0.6	51	51	204
0.6	+Inf	0	0	0

Table 5A: Vertical Feature Mask - Feature Type for Figure 13. Missing data is plotted white.

Feature Type	R	G	B
Clear air	0	38	255
Cloud	0	220	255
Aerosol	255	160	0
Stratospheric aerosol	250	255	0
Surface	0	255	110
Subsurface	192	192	192
Totally attenuated	0	0	0
No confidence cloud	200	60	230
No confidence aerosol	128	64	0

Table 6A: Vertical Feature Mask - Horizontal Averaging for Figure 14. Missing data is plotted white.

Horizontal Averaging	R	G	B
Background	202	202	255
1/3 km	244	104	12
1 km	0	255	0
5 km	255	255	0
20 km	0	125	63
80 km	0	0	128

Table 7A: Vertical Feature Mask - Ice/Water Phase for Figure 15. Missing data is plotted white.

Ice/Water Phase	R	G	B
Background	192	255	168
Unknown	255	0	0
Ice	255	255	255
Water	0	0	255
Oriented ice	169	169	169

Table 8A: Vertical Feature Mask - Aerosol Subtype for Figure 16. Missing data is plotted white.

Aerosol Subtype	R	G	B
Background	198	198	198
Marine	0	0	255
Dust	250	255	0
Polluted continental/smoke	255	179	0
Clean continental	0	166	0
Polluted dust	153	76	0
Elevated smoke	0	0	0
Dusty marine	0	142	194
PSC aerosol (stratospheric)	244	244	244
Volcanic ash (stratospheric)	138	138	138
Sulfate (stratospheric)	81	81	81
Unclassified (stratospheric)	121	45	148

Table 9A: Vertical Feature Mask - Cloud Subtype for Figure 17. Missing data is plotted white.

Cloud Subtype	R	G	B
Background	0	38	255
Low overcast, transparent	255	0	0
Low overcast, opaque	0	220	255
Transition stratocumulus	174	87	0
Low, broken cumulus	255	160	0
Alto cumulus (transparent)	250	255	0
Altostratus (opaque)	0	255	110
Cirrus (transparent)	192	192	192
Deep convective (opaque)	0	0	0